

Estimation of transverse bunch characteristics in the LHC using Schottky-based diagnostics

Kacper Lasocha^{1,2,*†} and Diogo Alves²

¹*Institute of Physics, Jagiellonian University, Kraków, Poland*

²*CERN, CH-1211 Geneva 23, Switzerland*

 (Received 11 February 2021; revised 6 April 2022; accepted 12 May 2022; published 3 June 2022)

In this paper, we discuss different approaches for the estimation of transverse bunch characteristics, namely, tune and chromaticity, using Schottky-based diagnostics. In particular, we show how, depending on the signal quality and the availability of other instruments or information sources, we can choose appropriate strategies combining both spectrum fitting procedures and explicit parameter calculations. In addition, we revisit and formally derive the expression that relates the chromaticity with the width of the Schottky spectral sidebands, discussing the rigorous meaning of this width and in which conditions it can be applied. Results obtained using the proposed approaches are compared with the standard techniques for different fills in the LHC.

DOI: [10.1103/PhysRevAccelBeams.25.062801](https://doi.org/10.1103/PhysRevAccelBeams.25.062801)

I. INTRODUCTION

Since the observation of Schottky signals at the Intersecting Storage Ring at CERN in 1971 [1], their analysis became an important noninvasive method for beam diagnostics. It has served as a tool for betatron tune, emittance, and chromaticity measurements at numerous accelerator facilities, including, among others, Relativistic Heavy Ion Collider at Brookhaven National Laboratory [2]; Tevatron and Recycler at Fermilab [3]; and heavy-ion synchrotron SIS-18 at GSI Helmholtzzentrum für Schwerionenforschung [4]. At CERN, Schottky diagnostics have successfully helped in the operation of Super Proton Synchrotron [5]; Antiproton Collector, Accumulator and Decelerator [6,7]; a new Extra Low Energy Antiproton ring [8]; and Large Hadron Collider (LHC) [9].

In Ref. [10], we have investigated how the transverse Schottky system in the LHC can be used for the estimation of longitudinal bunch characteristics, such as the bunch profiles or the synchrotron frequency distribution. It was shown that, in the absence of intrabunch coherent motion, the distribution of synchrotron amplitudes among all the particles in a bunch and the corresponding Schottky spectrum are related through a system of linear equations. The coefficients of these equations depend only on the

nominal synchrotron frequency if we consider the spectral region in the immediate vicinity of a harmonic of the revolution frequency. Both the amplitude distribution and the nominal synchrotron frequency can be found with the help of optimization algorithms such that this linear model fits the measured Schottky spectrum. If, on the other hand, one considers the transverse sidebands of the Schottky spectrum, then, in addition to the previous dependencies, also the betatron tune and the chromaticity play a role. Schottky diagnostics can, therefore, in principle, be used to provide chromaticity estimates without perturbing the beam, contrary to the popular rf-modulation technique, which requires measuring the tune while changing the beam momentum [11].

In this paper, we discuss different approaches aimed at obtaining noninvasive chromaticity and betatron tune estimates using a transverse Schottky system. Depending on the signal quality and the availability of external diagnostics or information sources, different strategies for combining spectrum fitting procedures and explicit parameter calculations may be adopted. Especially in the presence of spectral artifacts, such as coherent peaks or other distortions [12], the flexibility of being able to exclude affected regions from the analysis is of great practical relevance.

The paper is organized as follows. In Sec. II, we discuss the analytical expression for the transverse Schottky spectrum of bunched beams. Section III is devoted to betatron tune and chromaticity determination without spectral fitting. We shall call such procedures *explicit*. In Sec. III A, we propose a new method of finding the betatron tune, while in Sec. III B we discuss and confirm in a rigorous mathematical manner the well-known formula which connects chromaticity with the *width* of the

*kacper.lasocha@cern.ch

†Also at Institute of Physics, Jagiellonian University, Krakow, Poland.

Published by the American Physical Society under the terms of the Creative Commons Attribution 4.0 International license. Further distribution of this work must maintain attribution to the author(s) and the published article's title, journal citation, and DOI.

transverse sidebands. In particular, we show the rigorous mathematical meaning of this width. Section IV describes how both tune and chromaticity may be found from spectral fitting, as the natural extension of the method presented in Ref. [10]. In Sec. V, we present how the various proposed approaches can be combined and what factors have an impact on the choice of the most suitable strategy. In addition, we present and compare the chromaticity estimates obtained using the Schottky-based procedures proposed herein with the ones obtained experimentally using the rf-modulation method in the LHC. Closing remarks are present in Sec. VI.

In the scope of this article, we neglect the effects of octupole magnets, beam-beam effects, and beam interaction with the vacuum chamber. The primary domain of applicability of the Schottky diagnostics in the LHC is the ion (Pb^{82+}) beam at the injection energy, when the collisions have not yet started. All the experimental results presented in this paper have been acquired under such beam conditions, with octupole magnets switched off.

II. TRANSVERSE SCHOTTKY SPECTRUM

Let us recall the structure of a typical transverse Schottky spectrum which consists of two sidebands, symmetrically located on each side of a given harmonic of the revolution frequency ω_0 . The spectrum of each of these sidebands, due to a single particle, consists of a sequence of infinitely sharp Bessel satellites lined up in intervals of the particle's synchrotron frequency. The shape of the single-particle power spectral density (PSD) and its dependence on the value of chromaticity at LHC-like conditions is presented in Fig. 1. For clarity reasons, the frequency axis has been shifted down by a value of $(n-1) \cdot \omega_0/2\pi$, where $n = 427\,725$ is the harmonic of the revolution frequency observed by the LHC Schottky monitor and $\omega_0/2\pi \approx 11245.45$ Hz. As it follows, the LHC Schottky monitor operates at approximately 4.8 GHz.

In the presence of many particles with different synchrotron frequencies and random initial synchrotron and betatron phases, this set of infinitely sharp satellites interferes incoherently to form spectral structures, which eventually begin to overlap at high Bessel orders. The distance between the centers of the two transverse sidebands is exactly twice the value of the fractional part of the betatron tune. An example of the multiparticle PSD and its dependence on the value of chromaticity can be seen in Fig. 2.

Under the assumption of linear synchrotron oscillations which, as shown in Ref. [10], covers the overwhelming majority of LHC operating scenarios, the Schottky spectrum is described by an elegant analytical formula. We shall consider a single particle i , which is subject to betatron oscillations with a nominal tune $Q = Q_I + Q_F$ (where Q_I and Q_F are, respectively, the integer and the

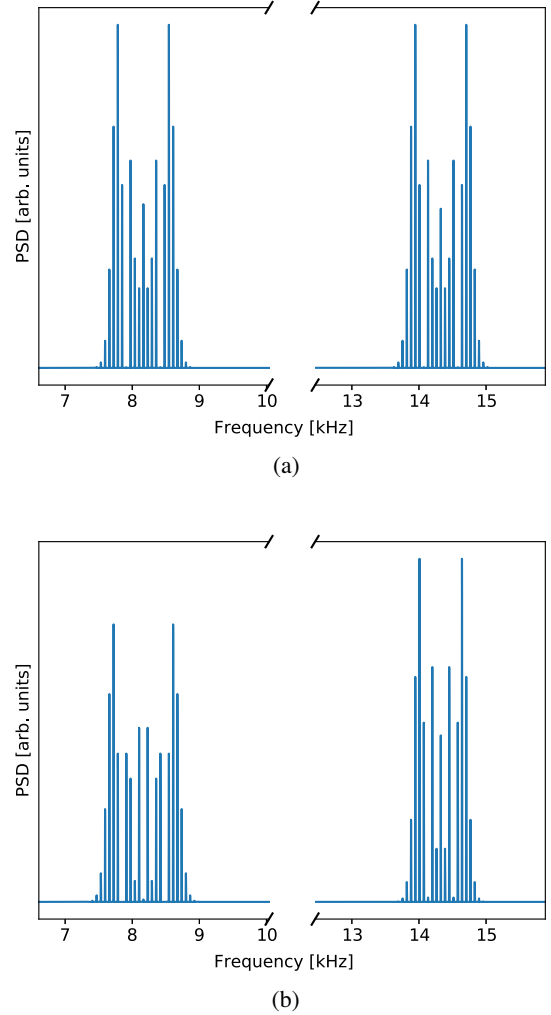


FIG. 1. Power spectral densities of a single particle's dipole moment, presented for two different values of chromaticity. Typical for the LHC values of synchrotron amplitude, frequency, and betatron tune are assumed. (a) $Q\xi = 0$ (b) $Q\xi = 20$.

fractional parts of the tune) and initial phase φ_{β_i} . Particle i is simultaneously performing synchrotron oscillations with amplitude $\hat{\tau}_i$, synchrotron frequency Ω_{s_i} , and initial phase φ_{s_i} . In addition, due to chromaticity $Q\xi$, the betatron tune oscillates with amplitude \widehat{Q}_i at the synchrotron frequency. The dipole moment signal due to a single particle i in the vicinity of the n th revolution harmonic can be written in the form

$$D^i(t) \propto \text{Re} \left(\sum_{p=-\infty}^{\infty} J_p(\chi_{i,n \mp Q_I}^{\pm}) e^{j\{t[(n \pm Q_F)\omega_0 + p\Omega_{s_i}] + \varphi_{\beta_i} + p\varphi_{s_i}\}} \right),$$

where $J_p(\cdot)$ is the Bessel function of the order of p and the \pm symbol denotes the summation over both signs. The argument of the Bessel function is given by

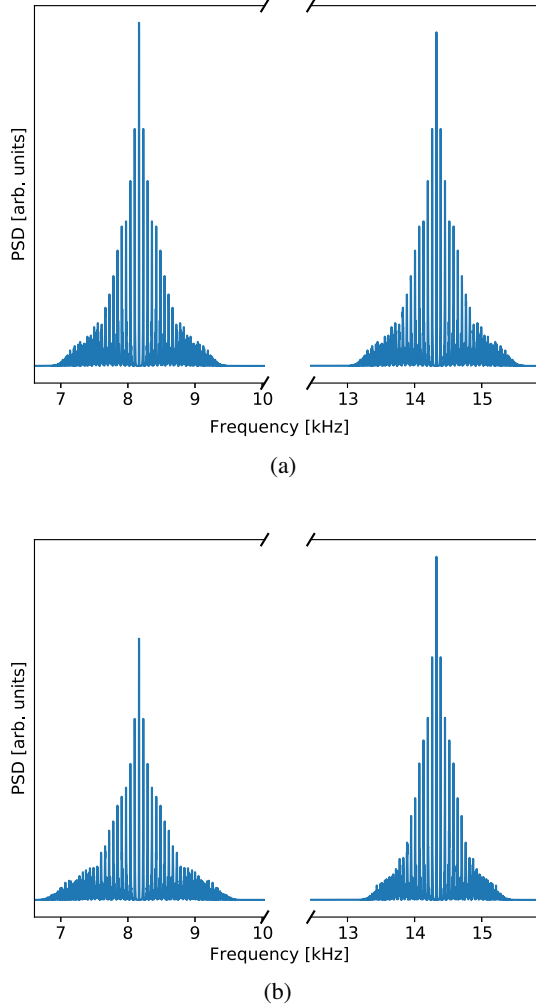


FIG. 2. Power spectral densities of the cumulative bunch dipole moment, presented for two different values of chromaticity. Typical for the LHC values of synchrotron frequency, betatron tune, and bunch profile are assumed. (a) $Q\xi = 0$ (b) $Q\xi = 20$.

$$\chi_{i,m}^{\pm} := \left(m\hat{\tau}_i \pm \frac{\hat{Q}_i}{\Omega_{s_i}} \right) \omega_0 = (m\eta \pm Q\xi) \frac{\omega_0 \hat{p}_i}{\Omega_{s_i} p_0},$$

where η is the slip factor, p_0 is the nominal momentum, and \hat{p}_i is the amplitude of momentum oscillations performed by particle i . The formal derivation of the previous expression for the dipole moment is presented in the Appendix. It has to be noted that this expression is slightly different from the one postulated in Refs. [13–15]; namely, the argument of the Bessel function differs by a value of $\eta Q \omega_0 \hat{p}_i / (\Omega_{s_i} p_0)$. This discrepancy comes from the two possible definitions for the betatron tune. In the scope of this paper, we adopt the convention that the betatron tune $Q_i(t)$ of particle i is defined with respect to the nominal revolution frequency ω_0 rather than the particle's own revolution frequency $\omega_i(t)$, as adopted by the other references. As a consequence, there are also two distinct definitions for chromaticity. The numerical difference between them, equal to ηQ ,

compensates for the additional $\eta Q \omega_0 \hat{p}_i / (\Omega_{s_i} p_0)$ term, so that the numerical value of the argument of the Bessel function remains the same.

The PSD of the single particle's dipole moment consists of two sidebands P_T^+ and P_T^- which, up to a scaling factor, are given by

$$P_T^{\pm}(\omega, \hat{\tau}_i) = \sum_{p=-\infty}^{\infty} J_p^2(\chi_{i,n \mp Q_i}^{\pm}) \delta[\omega - (n \pm Q_F)\omega_0 - p\Omega_{s_i}].$$

Writing the above formula as a function of $\hat{\tau}_i$ is justified by the fact that, in linear approximation of synchrotron motion, the synchrotron frequency Ω_{s_i} , the momentum amplitude \hat{p}_i , and the amplitude of betatron oscillation \hat{Q}_i are uniquely determined by the value of synchrotron amplitude (see the Appendix and Ref. [10]). In Ref. [10], we have shown that, under the assumption of no coherent intrabunch motion, the total PSD of the bunch current signal, $P_L(\omega)$, can be expressed by

$$P_L(\omega) = \sum_i P_L(\omega, \hat{\tau}_i) = \int_0^{\infty} g(\hat{\tau}) P_L^{\pm}(\omega, \hat{\tau}) d\hat{\tau},$$

where $g(\hat{\tau})$ is a probability density function of the synchrotron amplitudes among the particles and $P_L^{\pm}(\omega, \hat{\tau})$ is the current signal PSD of the single particle having synchrotron amplitude $\hat{\tau}$. By the exact same argumentation, we get an analogous result for the dipole moment, which reads

$$P_T^{\pm}(\omega) = \sum_i P_T^{\pm}(\omega, \hat{\tau}_i) = \int_0^{\infty} g(\hat{\tau}) P_T^{\pm}(\omega, \hat{\tau}) d\hat{\tau}, \quad (1)$$

where $P_T^{\pm}(\omega, \hat{\tau})$ is the single-particle dipole moment PSD of the particle having synchrotron amplitude $\hat{\tau}$. According to the previous formulas, it has the following form:

$$P_T^{\pm}(\omega, \hat{\tau}) = \sum_{p=-\infty}^{\infty} J_p^2(\chi_{\tau,n \mp Q_i}^{\pm}) \delta[\omega - (n \pm Q_F)\omega_0 - p\Omega_s(\hat{\tau})], \quad (2)$$

with the argument of the Bessel function given by

$$\chi_{\tau,m}^{\pm} := \left(m\hat{\tau} \pm \frac{\hat{Q}(\hat{\tau})}{\Omega_s(\hat{\tau})} \right) \omega_0 = (m\eta \pm Q\xi) \frac{\omega_0 \hat{p}(\hat{\tau})}{\Omega_s(\hat{\tau}) p_0}. \quad (3)$$

In fact, due to the additional betatron phase in the exponent of the expression of the dipole moment, and unlike in Ref. [10], Eq. (1) remains valid even in the case of coherent synchrotron motion. It is enough to have either the initial synchrotron or betatron phases uniformly distributed. Furthermore, in the latter case, and again unlike in

Ref. [10], we no longer have to exclude the $p = 0$ Bessel satellite from our analysis as it now adds up incoherently.

It is important to underline that Eq. (1) describes the expected value of the instantaneous Schottky spectrum. The time average of the experimentally measured spectra approximates this expected value. The incoherent spectrum, however, will always be subject to intrinsic random fluctuations. In addition, as will be seen in the following sections, spurious components whose origin is yet unknown to the authors may pollute the spectra. These components need to be treated differently in the analysis.

III. EXPLICIT PARAMETER ESTIMATION

A. Betatron tune

According to the theory recalled in the previous section, each of the transverse sidebands should be symmetric. The axis of symmetry coincides with the p -zero Bessel satellite, for which the frequency is equal to $(n \pm Q_F)\omega_0$. Hence, detection of this satellite enables us to determine the tune value.

Analyzing previously proposed methods of Schottky-based tune measurements [9,16,17], we can group them into two types. The first is based on peak detection, followed by the estimation of which peak is most likely the p -zero satellite. One considered feature is the height; however, there is no guarantee that the central satellite has the highest power. Alternatively, the overall shape of the transverse sideband is considered, and, by means such as curve fitting or weight averaging, the center of the sideband is determined, even if it does not correspond to a local maximum. The biggest drawback of this approach is poor robustness to nonsymmetric shapes of the sidebands.

We propose a new method of tune calculation, which we call the mirrored difference (MD) method. It exploits the observation that, even in cases where the overall shape of the transverse hump is distorted, we still observe correlation between the power of the corresponding positive and negative Bessel p satellites. We define, therefore, a cost function as

$$C_{MD}(m) = \sum_{i=1}^{i=N} |P_T^{\pm}(\omega_{m-i}) - P_T^{\pm}(\omega_{m+i})|, \quad (4)$$

where $P_T^{\pm}(\omega_n)$ is the power of n th point in the spectrum and N is the range parameter, which should correspond to the expected sideband width. The value of m which minimizes the above cost function indicates the frequency bin of $(n \pm Q_F)\omega_0$. In addition, a supplementary check can be performed by confirming that the detected frequency bin is indeed a local maximum. This can be simply done by comparing the value of $P_T^{\pm}(\omega_n)$ with the average power in the sideband. That should be enough, as it immediately excludes the valleys in between satellites, leaving only the local maxima as possible points of symmetry. Finally,

interpolation techniques can be used in order to increase point density in the spectrum and decrease C_{MD} even more. It should be noted that the presence of irregularities or artifacts outside the central region of the sideband affects nearly all the summands in Eq. (4) in a comparable way. As a result, an additional artificial peak cannot "drag" the calculated tune toward itself, unless its power is so large that its location minimizes the cost function despite the induced asymmetry.

B. Chromaticity

There exists in the literature [3,9,17–19] a well-known formula which relates the width of the transverse sidebands to the value of chromaticity:

$$Q\xi = -\eta \left(n \frac{\Delta f_- - \Delta f_+}{\Delta f_- + \Delta f_+} - Q_I \right), \quad (5)$$

where by Δf_- and Δf_+ we denote, respectively, the width of the left and right sidebands and n , as previously, denotes the observed harmonic of the revolution frequency. Depending on the adopted definition of tune (see discussion in Sec. II), the formula with the $+Q_F$ term instead of $-Q_I$ is also given. However, since normally we have $n \gg Q$, this does not lead to significant discrepancies.

In the case of a coasted beam, an analogous formula can be derived straightforwardly from the works of Boussard [15] and van der Meer [20]. The result in the case of bunched beams was justified by the assumption that $J_p(x) \approx 0$ for $p > x$ [3], which is only approximately correct, especially in the case of small x . As far as the authors know, it was never shown that the result holds, in general, or what the exact mathematical meaning is of the widths, Δf_- and Δf_+ , of the sidebands. One could, for example, use the rms width, the standard deviation of a fitted Gaussian, or even the width measured at some power threshold. Furthermore, all of these can be calculated in either linear or logarithmic (dB) scale. In fact, a few different approaches can be found in the available literature [9,19,21]. In the following, we shall provide a formal derivation of Eq. (5) for the case of bunched beams and clarify that these widths should be defined as the rms widths of the transverse sidebands in linear scale. By rms width, we mean the standard deviation of the PSD sideband, if treated as a histogram. This is defined by an integral over the frequency range containing the whole sideband, where the integrand is the power spectral density multiplied by the squared distance to the sideband's center. The rms width of the transverse sideband can be calculated using Eqs. (1) and (2). As we know that the sideband is centered on the frequency $(n \pm Q_F)\omega_0$, we derive the rms width by calculating the variance:

$$\begin{aligned} \sigma_{\pm}^2 &= \int P_T^{\pm}(\omega) [\omega - (n \pm Q_F)\omega_0]^2 d\omega \\ &= \iint_0^{\infty} g(\hat{\tau}) P_T^{\pm}(\omega, \hat{\tau}) [\omega - (n \pm Q_F)\omega_0]^2 d\hat{\tau} d\omega. \end{aligned}$$

We can now substitute $P_{\mp}^{\pm}(\omega, \widehat{\tau})$, using Eq. (2), and obtain

$$\begin{aligned}\sigma_{\pm}^2 &= \iint_0^{\infty} g(\widehat{\tau}) \sum_{p=-\infty}^{\infty} J_p^2(\chi_{\widehat{\tau}, n \mp Q_I}^{\pm}) \delta[\omega - (n \pm Q_F)\omega_0 - p\Omega_s(\widehat{\tau})][\omega - (n \pm Q_F)\omega_0]^2 d\widehat{\tau} d\omega \\ &= \int_0^{\infty} \int g(\widehat{\tau}) \sum_{p=-\infty}^{\infty} J_p^2(\chi_{\widehat{\tau}, n \mp Q_I}^{\pm}) \delta[\omega - (n \pm Q_F)\omega_0 - p\Omega_s(\widehat{\tau})][\omega - (n \pm Q_F)\omega_0]^2 d\omega d\widehat{\tau} \\ &= \int_0^{\infty} g(\widehat{\tau}) \sum_{p=-\infty}^{\infty} J_p^2(\chi_{\widehat{\tau}, n \mp Q_I}^{\pm}) [p\Omega_s(\widehat{\tau})]^2 d\widehat{\tau} = \int_0^{\infty} g(\widehat{\tau}) \left(\sum_{p=-\infty}^{\infty} J_p^2(\chi_{\widehat{\tau}, n \mp Q_I}^{\pm}) p^2 \right) \Omega_s(\widehat{\tau})^2 d\widehat{\tau}.\end{aligned}$$

Previously, we have allowed ourselves to change the integration order using a version of the Fubini-Tonelli theorem which holds for generalized functions (see Chap. 4 in Ref. [22]). Now we can use the expression [see Formula (2.3) in Ref. [23]]

$$\sum_{p=-\infty}^{\infty} J_p^2(x) p^2 = \frac{x^2}{2}$$

and get

$$\sigma_{\pm}^2 = \int_0^{\infty} g(\widehat{\tau}) \frac{(\chi_{\widehat{\tau}, n \mp Q_I}^{\pm})^2}{2} \Omega_s(\widehat{\tau})^2 d\widehat{\tau}.$$

Substituting $\chi_{\widehat{\tau}, n \mp Q_I}^{\pm}$, as given in Eq. (3), we have that

$$\begin{aligned}\sigma_{\pm}^2 &= \int_0^{\infty} g(\widehat{\tau}) \frac{\left([(n \mp Q_I)\eta \pm Q\xi] \frac{\omega_0 \widehat{p}(\widehat{\tau})}{\Omega_s(\widehat{\tau}) p_0} \right)^2}{2} \Omega_s(\widehat{\tau})^2 d\widehat{\tau} \\ &= [(n \mp Q_I)\eta \pm Q\xi]^2 \int_0^{\infty} g(\widehat{\tau}) \left(\frac{\omega_0 \widehat{p}(\widehat{\tau})}{2\Omega_s(\widehat{\tau}) p_0} \right)^2 \Omega_s(\widehat{\tau})^2 d\widehat{\tau} \\ &= [(n \mp Q_I)\eta \pm Q\xi]^2 \cdot C,\end{aligned}$$

where $C = \int_0^{\infty} g(\widehat{\tau}) \left(\frac{\omega_0 \widehat{p}(\widehat{\tau})}{2\Omega_s(\widehat{\tau}) p_0} \right)^2 \Omega_s(\widehat{\tau})^2 d\widehat{\tau}$ is a positive constant.

At this point, it is necessary to note that, although $\sigma_{\pm} := \sqrt{\sigma_{\pm}^2}$ is by definition positive, the value of $[(n \mp Q_I)\eta \pm Q\xi]$ can be of any sign. One can distinguish two cases: 1. $[(n - Q_I)\eta + Q\xi]$ and $[(n + Q_I)\eta - Q\xi]$ are both positive or both negative; 2. $[(n - Q_I)\eta + Q\xi]$ and $[(n + Q_I)\eta - Q\xi]$ have opposite signs. For high enough values of n , only the first option remains possible. In the case of the LHC Schottky monitor $n = 427725$, $Q_I = 59$ or 64 , and $\eta \approx -3.182 \times 10^{-4}$, which results in $(n \pm Q_I)\eta \approx -136$, to be compared with $Q\xi$ values ranging usually from -20 to 20 . Under this assumption, it is straightforward to check

that, if one takes $\Delta f_- = \sigma_-$ and $\Delta f_+ = \sigma_+$, then constant C cancels out in Eq. (5) and one gets

$$\begin{aligned}& -\eta \left(n \frac{\Delta f_- - \Delta f_+}{\Delta f_- + \Delta f_+} - Q_I \right) \\ &= -\eta \left(n \frac{[(n + Q_I)\eta - Q\xi] - [(n - Q_I)\eta + Q\xi]}{[(n + Q_I)\eta - Q\xi] + [(n - Q_I)\eta + Q\xi]} - Q_I \right) \\ &= -\eta \left(n \frac{2Q_I\eta - 2Q\xi}{2n\eta} - Q_I \right) = -\eta \left(Q_I - \frac{Q\xi}{\eta} - Q_I \right) = Q\xi.\end{aligned}$$

If, however, the considered harmonic of the revolution frequency is low, one might have that $[(n \mp Q_I)\eta \pm Q\xi]$ are of opposite signs, and Eq. (5) should be replaced with

$$Q\xi = -\eta \left(n \frac{\Delta f_- + \Delta f_+}{\Delta f_- - \Delta f_+} - Q_I \right). \quad (6)$$

Unfortunately, as it is very likely that in such a case the sign of $[(n \mp Q_I)\eta \pm Q\xi]$ strictly depends on the value of $Q\xi$, which is to be determined, the correction introduced by Eq. (6) is of a very limited practical use.

We have, therefore, rigorously proven Eq. (5) under the assumption that $\Delta f_- = \sigma_-$ and $\Delta f_+ = \sigma_+$, with σ_{\pm} calculated using linear scale PSD values and for a sufficiently high value of the revolution frequency harmonic n . Simple algebraic manipulation shows that, if any other interpretation of the width $\widetilde{\Delta f}_{\pm}$ would also result in the correct value of chromaticity, it has to be in the relation $\widetilde{\Delta f}_{\pm} = \alpha \Delta f_{\pm}$, where α is a nonzero scaling factor, the same for both upper and lower sidebands.

IV. SPECTRUM FITTING PROCEDURES

In Ref. [10], we have shown that the discrete Fourier transform (DFT) of the longitudinal part of the Schottky spectrum can be expressed as

$$\underbrace{\begin{bmatrix} P_{DFT}(\omega_1, \hat{\tau}_1, \Omega_{s_0}) & \cdots & P_{DFT}(\omega_1, \hat{\tau}_n, \Omega_{s_0}) \\ P_{DFT}(\omega_2, \hat{\tau}_1, \Omega_{s_0}) & \cdots & P_{DFT}(\omega_2, \hat{\tau}_n, \Omega_{s_0}) \\ \vdots & \ddots & \vdots \\ P_{DFT}(\omega_m, \hat{\tau}_1, \Omega_{s_0}) & \cdots & P_{DFT}(\omega_m, \hat{\tau}_n, \Omega_{s_0}) \end{bmatrix}}_{\mathcal{M}(\Omega_{s_0})} \cdot \underbrace{\begin{bmatrix} \tilde{g}(\hat{\tau}_1) \\ \tilde{g}(\hat{\tau}_2) \\ \vdots \\ \tilde{g}(\hat{\tau}_n) \end{bmatrix}}_{\mathcal{A}} = \underbrace{\begin{bmatrix} P_{DFT}(\omega_1) \\ P_{DFT}(\omega_2) \\ \vdots \\ P_{DFT}(\omega_m) \end{bmatrix}}_{\mathcal{S}}, \quad (7)$$

where the columns of matrix $\mathcal{M}(\Omega_{s_0})$ correspond to the spectra of a single particle with synchrotron amplitude $\hat{\tau}_i$ and nominal synchrotron frequency Ω_{s_0} , vector \mathcal{A} represents the discrete approximation of the distribution of synchrotron amplitudes, and vector \mathcal{S} is the DFT estimate of the bunch PSD, which can be compared with the experimentally obtained Schottky spectrum. In the case of the transverse Schottky sidebands, and as was seen in Sec. II, we need to include two additional parameters, betatron tune and chromaticity, so that the new matrix equation reads

$$\underbrace{\begin{bmatrix} P_{DFT}^{T,\pm}(\omega_1, \hat{\tau}_1, \Omega_{s_0}, Q, Q\xi) & \cdots & P_{DFT}^{T,\pm}(\omega_1, \hat{\tau}_n, \Omega_{s_0}, Q, Q\xi) \\ P_{DFT}^{T,\pm}(\omega_2, \hat{\tau}_1, \Omega_{s_0}, Q, Q\xi) & \cdots & P_{DFT}^{T,\pm}(\omega_2, \hat{\tau}_n, \Omega_{s_0}, Q, Q\xi) \\ \vdots & \ddots & \vdots \\ P_{DFT}^{T,\pm}(\omega_m, \hat{\tau}_1, \Omega_{s_0}, Q, Q\xi) & \cdots & P_{DFT}^{T,\pm}(\omega_m, \hat{\tau}_n, \Omega_{s_0}, Q, Q\xi) \end{bmatrix}}_{\mathcal{M}(\Omega_{s_0}, Q, Q\xi)} \cdot \underbrace{\begin{bmatrix} \tilde{g}(\hat{\tau}_1) \\ \tilde{g}(\hat{\tau}_2) \\ \vdots \\ \tilde{g}(\hat{\tau}_n) \end{bmatrix}}_{\mathcal{A}} = \underbrace{\begin{bmatrix} P_{DFT}^{T,\pm}(\omega_1) \\ P_{DFT}^{T,\pm}(\omega_2) \\ \vdots \\ P_{DFT}^{T,\pm}(\omega_m) \end{bmatrix}}_{\mathcal{S}}. \quad (8)$$

The left-hand sides of the previous two equations can be interpreted as models which, given the correct set of parameters, should, in principle, make \mathcal{S} match the experimentally measured spectra. Inverting the problem, and given an experimental spectrum, we may try to fit these parameters in such a way that the resulting model predicts a spectrum \mathcal{S} that coincides with the measured one. The number of considered synchrotron amplitudes has to be smaller than number of the spectrum frequency bins, as otherwise the problem would be ill posed, and as in Ref. [10] we take 50 distinct amplitudes in our analyses. The number of considered frequency bins varies, as will be explained in the next section, and is in range between 1932 and 6056 bins. In order to determine the correct values of Ω_{s_0} , Q , $Q\xi$, and \mathcal{A} we look for values that minimize the following cost function:

$$C(\Omega_{s_0}, Q, Q\xi, \mathcal{A}) = |\log[\mathcal{M}(\Omega_{s_0}, Q, Q\xi) \cdot \mathcal{A}] - \log[\mathcal{S}_{\text{exp}}]|^2. \quad (9)$$

The log functions are taken pointwise, and $|\cdot|$ is the standard Euclidean norm. We have decided here to take a logarithm of the measured and simulated spectrum in order to be more sensitive to the low-magnitude spectral peripheries and more robust to noise, as it was observed that the noise level in the spectrum is proportional to the spectrum value.

As discussed in Ref. [10], we use the Rice distribution [24] to parametrize the distribution of synchrotron amplitudes. This reduces the problem of estimating the \mathcal{A} vector down to determining no more than two parameters of a Rice

distribution. The minimization of the cost function may be performed using, for example, one of the many optimizing routines provided by the SciPy library [25]. In the scope of this paper, the bound-constrained limited-memory BFGS method [26] was used.

A great advantage of spectrum fitting procedures is that one is free to choose the range of used frequencies $(\omega_1, \dots, \omega_n)$. That means that, if for any reason we need to exclude part of the spectrum from our analysis, we can still perform a fit and estimate the desired quantities. In the process of fitting, all parameters Ω_{s_0} , Q , $Q\xi$, and \mathcal{A} are taken into account. However, not all of them necessarily have to be fitted. If any of them is known *a priori*, it can be taken as a constant parameter, not subject to any change. Such an approach can considerably decrease the calculation time and improve fitting precision.

V. ESTIMATION OF BUNCH CHARACTERISTICS

Equation (7) tells us that the overall shape of the longitudinal Schottky spectrum is determined by the nominal synchrotron frequency and the distribution of synchrotron amplitudes, while for the case of the transverse sidebands one has to consider, in addition to the previous, also the contribution of the betatron tune and the chromaticity [see Eq. (8)]. One can, therefore, envisage as possible the derivation of these quantities using a fitting approach. Some of them, namely, the betatron tune and the chromaticity, could also, in principle, be obtained from the Schottky spectrum without using a fitting procedure, as

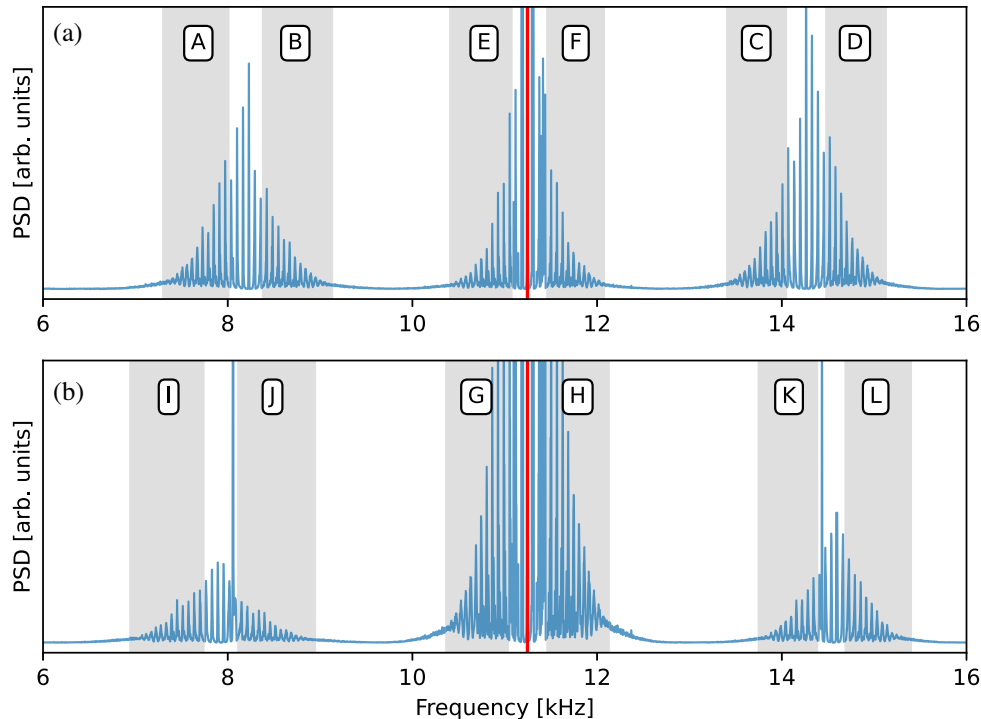


FIG. 3. Gray shaded regions show the frequency ranges used in the fitting procedure of the horizontal (a) and the vertical (b) Schottky spectra for LHC fill 7435. The red vertical line denotes the harmonic of the revolution frequency.

explained in Sec. III. In Ref. [10], we have shown that, under the assumption of no intrabunch coherent motion, the distribution of synchrotron amplitudes can be derived from the longitudinal bunch profile, and vice versa. The nominal synchrotron frequency can, if needed, also be obtained from other diagnostics or from calculations based on rf system parameters [27,28].

We can see that there exists a surplus in the number of procedures. On the other hand, this surplus can be used either as a cross-check or as a way to improve the fitting quality by providing external constant parameters and reducing the number of parameters to be fit. It is important to note that all fitting procedures have to take into account all the parameters which have an impact on the spectrum. These have to either be fitted or provided as a constant parameter.

Although mentioned methods may be intermingled in many possible ways, we will present only a subset of combinations, which we believe gives a good overview of most of the use cases. These scenarios will be benchmarked using experimental Schottky data taken during LHC run 2. The dataset consists of horizontal and vertical measurements taken at injection energy during three different fills: 7435, 7443, and 7486. Data from both LHC rings are analyzed. For fill 7435 we analyze beam 1 data, while for fills 7443 and 7486 we focus on beam 2.

As previously mentioned, fitting procedures do not require taking the whole Schottky spectrum into consideration. We shall demonstrate this feature by performing a

single fit on a subset of frequencies, as shown, for example, in Fig. 3, where we can see that the strong coherent peaks located in both transverse sidebands of the spectrum coming from the vertical Schottky system (left to the region J and right to the region K) have been conveniently excluded from the selected regions. The integrated power of the experimental and simulated spectra are normalized in each spectral window so that we do not need to fit additional gain parameters corresponding to the linear scaling of longitudinal and transverse sidebands.

The results presented in this section are organized as follows. Each distinct scenario representing a different analysis method is described in an independent subsection. If the scenario involves fitting, the fitting results are presented separately for every region marked in Fig. 3. In order to reduce the number of plots, only the fits corresponding to fill 7443 are presented. In the last subsection, we present a comparison between the chromaticity estimates obtained for each scenario with the chromaticity estimates obtained with the standard rf-modulation technique.

A. First scenario

In theory, both the betatron tune and the chromaticity could be calculated based on methods presented in Sec. III. It requires, however, a signal of very good quality, as we are not able to exclude any part of the spectrum. In addition, the unavoidable presence of noise, and especially of coherent

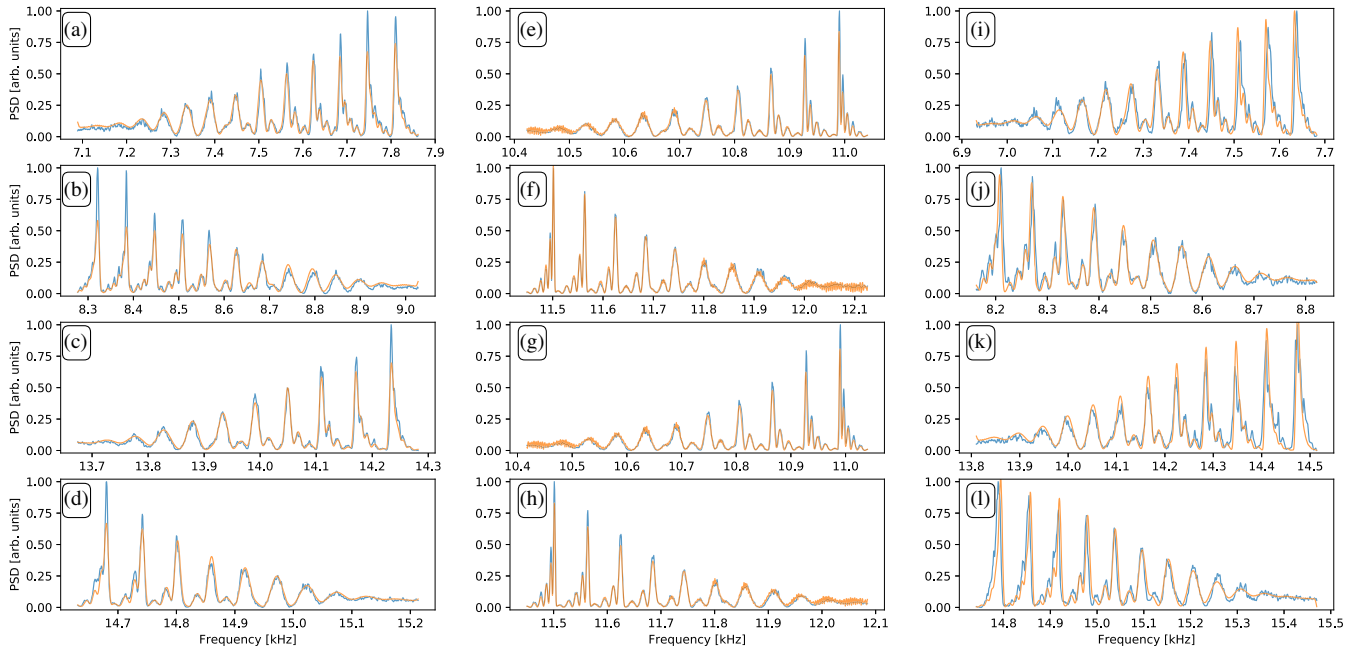


FIG. 4. Measured (blue lines) transverse and longitudinal Schottky spectrum for LHC fill 7443, compared with the best fitted spectrum (orange lines) obtained from the second scenario strategy. A–L region labels correspond to frequency ranges equivalently located as shown in Fig. 3 for fill 7435.

spectral peaks, can have a very strong impact on the rms widths of transverse sidebands, thus causing errors in the calculated chromaticity.

B. Second scenario

In most cases, at least in the LHC, chromaticity cannot be accurately calculated using Eq. (5). In such cases, we have to fit the transverse sidebands, or a subset of them, according to the procedure discussed in Sec. IV. In order to further constrain the solution space to a plausible region, it is sometimes desirable to fit as few parameters as possible. We assume that the nominal synchrotron frequency is known, either through the precise knowledge of rf parameters or from external diagnostics. We estimate the value of the betatron tune directly from the Schottky spectrum, according to the procedure described in Sec. III A. This method has proven to be very robust and can be applied in most of the cases. Knowing the nominal synchrotron frequency, we can determine the distribution of synchrotron amplitudes from fitting the longitudinal portion of the Schottky spectrum. Finally, only chromaticity is left to be determined through transverse fitting or, in this case, simply scanning. A comparison between the experimental and fitted spectrum, for the different frequency regions, is shown in Fig. 4.

C. Third scenario

In certain circumstances [29], it may happen that we simply cannot fit the longitudinal part of the Schottky spectrum. Furthermore, it can also happen that no useful

information is available from external devices. In such cases, we can rely on only the information contained in the transverse sidebands of the Schottky spectrum. A comparison between the experimental and fitted spectrum, for the different frequency regions, is shown in Fig. 5.

D. Fourth scenario

The last considered scenario can be seen as an enhanced version of the third scenario. Again, we fit all the parameters, apart from the betatron tune, within a single fitting routine. This time, however, we fit simultaneously both the longitudinal and the transverse portions of the Schottky spectrum. In case we have a reliable longitudinal spectral region, this scenario has a clear advantage over the third scenario, as it provides more constraints on the fitted parameters. It also represents the most straightforward approach for the simultaneous estimation of all parameters given the entire set of available data. A comparison between the experimental and fitted spectrum is shown in Fig. 6.

E. Results

For all the considered scenarios and fills, we present here the results of the chromaticity estimates. Every estimate is performed separately for each plane. As a comparison, we present also the chromaticity calculated from the rf-modulation technique. The analyzed spectra were acquired before the start of the rf modulation to avoid the strong spectral distortions caused by it. For that reason, only a “fairly close-in-time” comparison is possible, as seen from

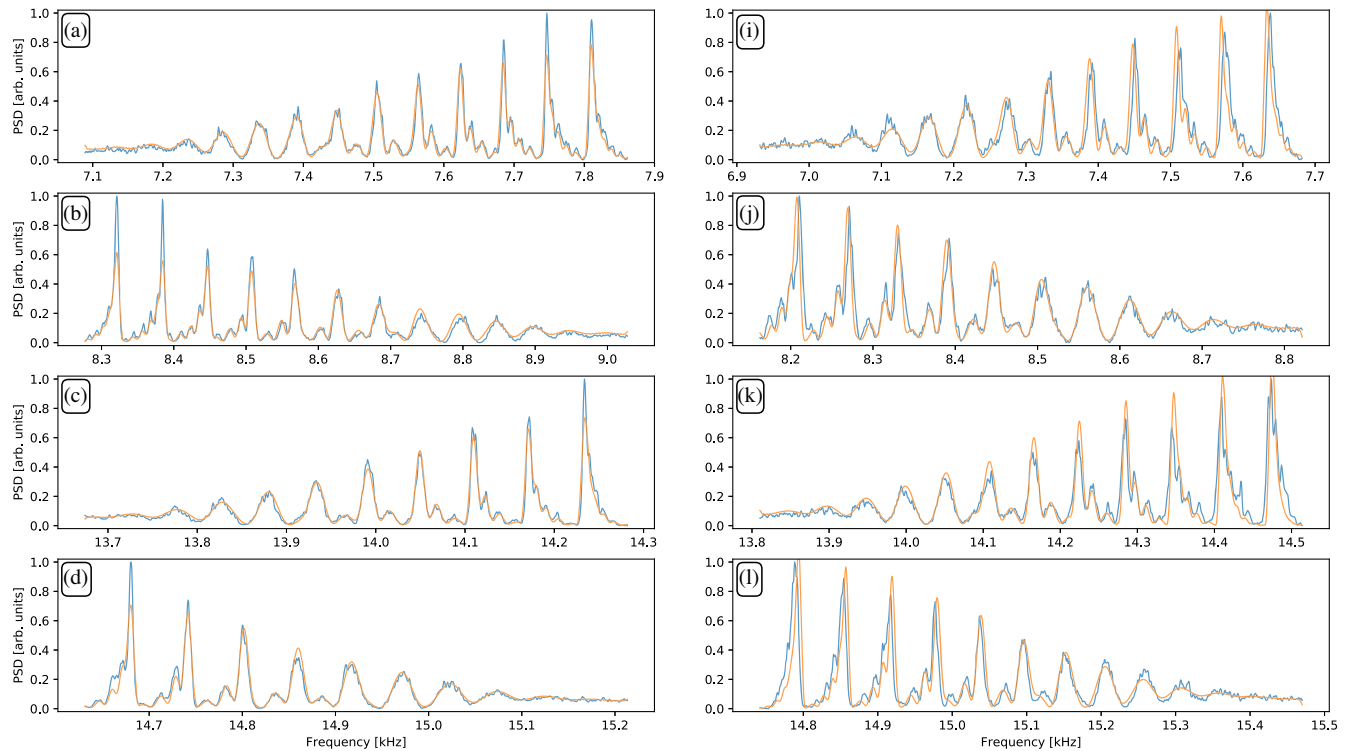


FIG. 5. Measured (blue lines) transverse Schottky spectrum for LHC fill 7443, compared with the best fitted spectrum (orange lines) obtained from the third scenario strategy. A–D and I–L region labels correspond to frequency ranges equivalently located as shown in Fig. 3 for fill 7435.

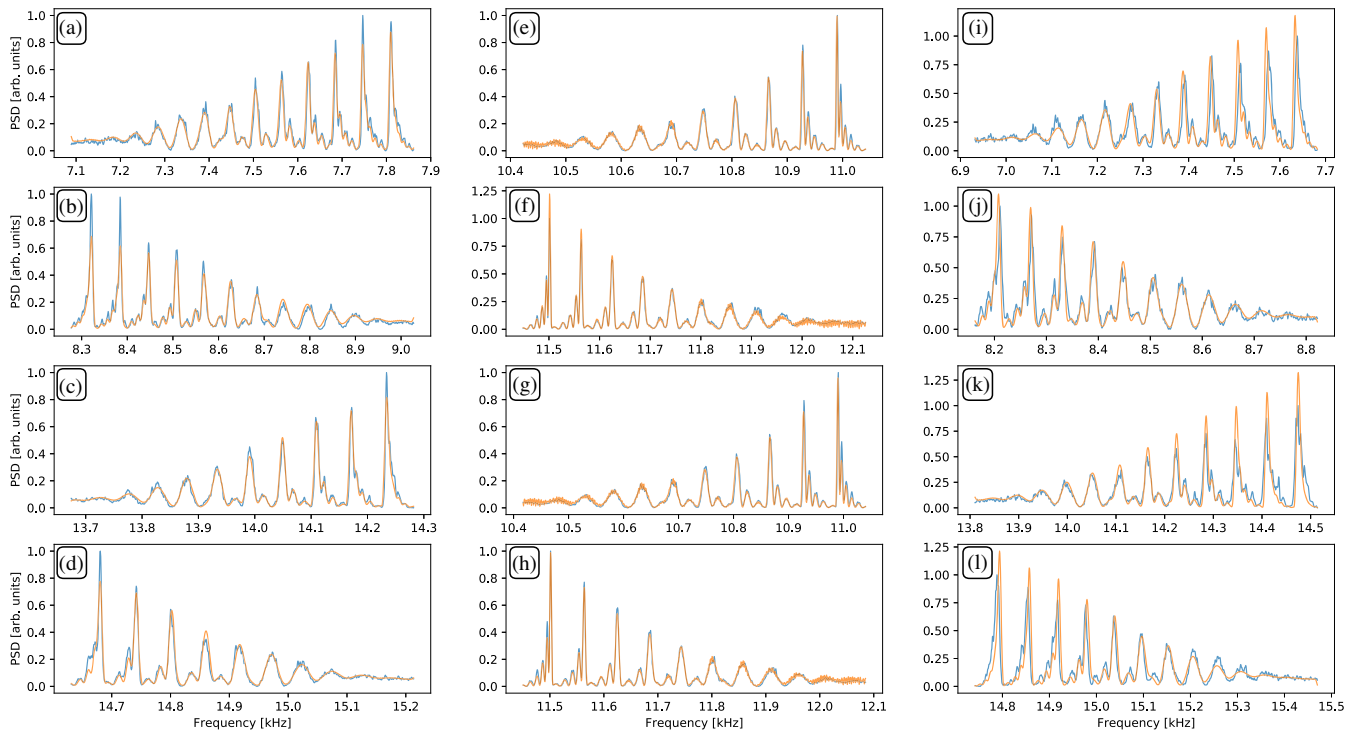


FIG. 6. Measured (blue lines) longitudinal and transverse Schottky spectrum for LHC fill 7443, compared with the best fitted spectrum (orange lines) obtained from the fourth scenario strategy. A–L region labels correspond to frequency ranges equivalently located as shown in Fig. 3 for fill 7435.

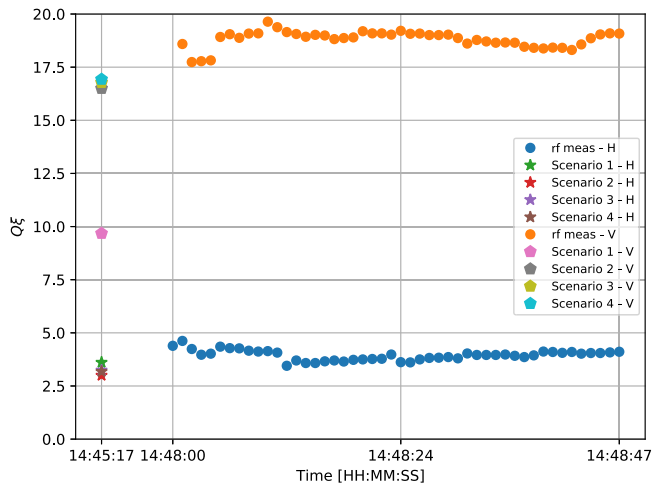


FIG. 7. Chromaticity measurements during LHC fill 7435.

the x axis in Figs. 7–9. However, it is important to note that during all the time windows presented in these plots there was no change in the current of the sextupole magnets, indicating that the values of chromaticity should remain constant.

Analyzing these plots, we may conclude that the results obtained with scenarios 2–4 are self-consistent and strongly correlated with rf-modulation measurements. Chromaticity values calculated using the first scenario are less robust, as can be observed especially from the results of fill 7486 horizontal and fill 7435 vertical. Such a lack of robustness can be understood, for example, if we take a look at Fig. 3. Two strong coherent peaks are present in the vertical spectrum, just behind the right border of region K and left border of region J. These peaks have to be included in the calculations, hence causing Eq. (5) to fail. The exact same problem was verified for the case of fill 7486 horizontal. For scenarios 2–4, as previously highlighted, we can exclude such distorted spectral regions and obtain better and plausible results.

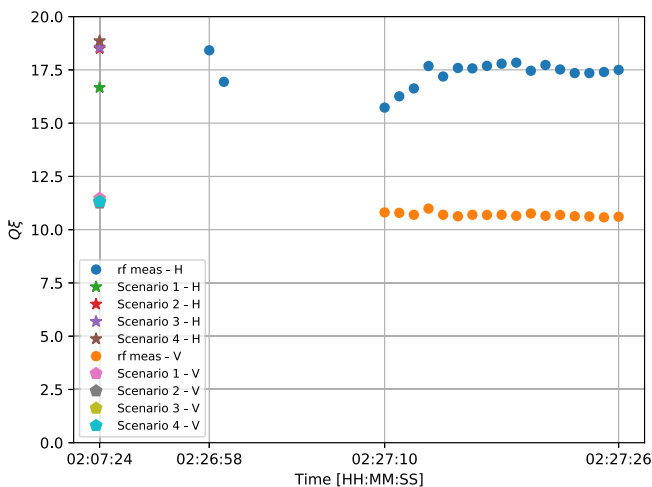


FIG. 8. Chromaticity measurements during LHC fill 7443.

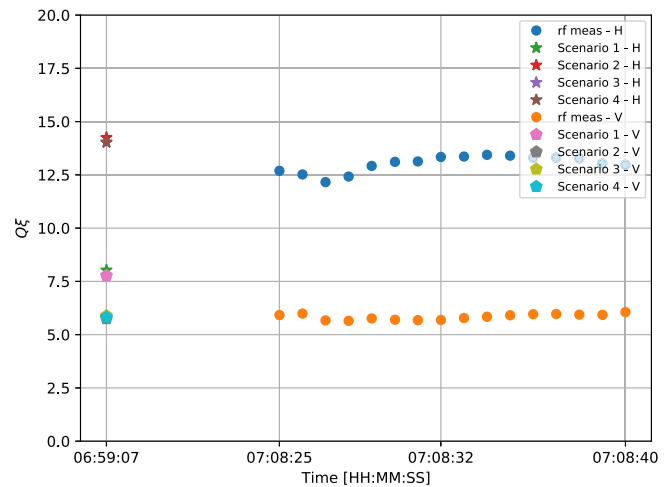


FIG. 9. Chromaticity measurements during LHC fill 7486.

The question remains of whether the accuracy of the chromaticity estimates is sufficient. The difference between the chromaticity value estimations provided by the proposed approaches and the rf-modulation technique is sometimes greater than a unit. It is, however, important to note that the spread of the presented rf-modulation results is not negligible and happens to cover several units. Taking this into account, the noninvasive methods presented here are shown to provide chromaticity estimates which are at least comparable to the ones obtained from the rf-modulation technique.

In order to understand the limitations of the Schottky-based chromaticity estimation methods presented herein, we should assess the sensitivity of the spectrum itself with respect to chromaticity. Such an exercise is preliminarily illustrated in Fig. 10. It is worth noting how subtle the changes in the spectrum are for different values of

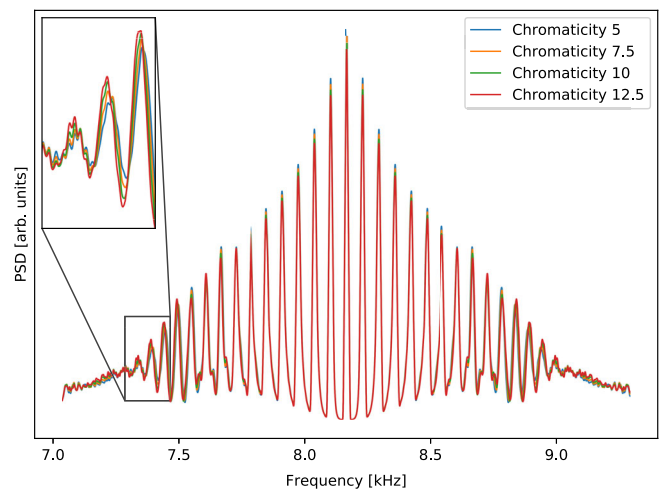


FIG. 10. Simulated lower transverse Schottky sidebands for different values of chromaticity. Bunch profile and synchrotron frequency as in fill 7435.

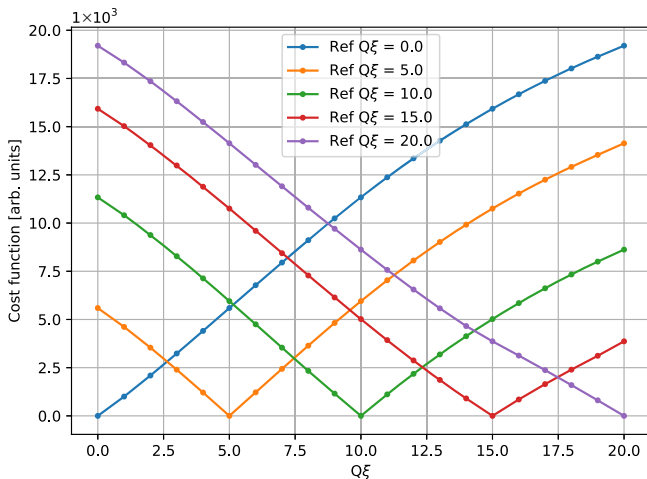


FIG. 11. Difference between spectra of a typical LHC bunch for different values of chromaticity expressed in terms of cost function (9).

chromaticity and how challenging this distinction can be when dealing with real-life Schottky spectra.

We may also note, from Figs. 7–9, that the chromaticity estimates seem to be more precise and also to agree more with the estimates from the rf-modulation technique, for lower values of chromaticity. In Fig. 11, we can see that the value of the cost function Eq. (9), applied this time not to the theoretical and experimental spectra but to two theoretical ones, of chromaticities, respectively, $Q\xi = 5$ and $Q\xi = 7$ is the same as the one for spectra with chromaticities $Q\xi = 15$ and $Q\xi = 18$. This observation, verified to hold for various types of LHC-like profiles, is not necessarily true for shorter bunches.

In all proposed scenarios, the value of betatron tune is calculated with the MD method, described in Sec. III A. The high precision of the method is confirmed by the fact that all the fitted spectra are correctly located with respect

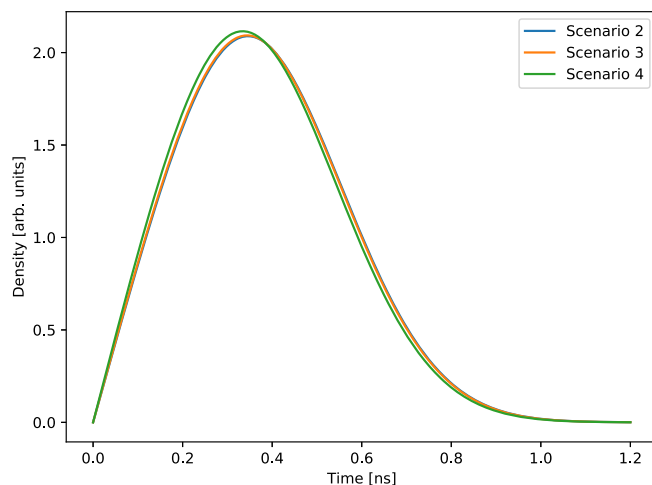


FIG. 12. Distribution of synchrotron amplitudes during LHC fill 7443, obtained by following different strategies.

to the experimental ones. Any deviations would result in an evident misalignment.

As a final sanity check, distributions of synchrotron amplitudes obtained by following scenarios 2–4 might be compared. Such an example is shown in Fig. 12, confirming self-consistency of presented approaches and compares well with a typical LHC bunch length of 1–1.2 ns.

VI. CONCLUSIONS

The aim of this paper is to revisit, improve, and develop new methods for transverse Schottky analysis with special emphasis on noninvasive chromaticity estimates in the LHC. From a theoretical point of view, the most important contribution of this work is the formal derivation of the relationship between the natural chromaticity and the rms widths of the transverse sidebands in the case of a bunched beam. This derivation provides an exact and unambiguous definition for the sideband widths often used to estimate chromaticity.

Considering the practical aspects, we have proposed a new algorithm for explicit tune calculation. We have shown as well that the matrix formalism introduced in Ref. [10] for the longitudinal part of the spectrum may be extended as well in order to analyze the transverse part. Moreover, we have studied how the different types of analyses can interplay and under what circumstances they can be used. Finally, we have discussed the sensitivity of the Schottky spectrum to chromaticity, as a step toward deep understanding of the fundamental limitations of Schottky signal analysis.

The obtained results are self-consistent and compare well with the reference measurements. Good spectral fits were clearly shown in Fig. 4–6, where it can be seen that not only the overall shape of the spectrum is recovered, but also the internal structure of the synchrotron satellites is extremely well reproduced.

As a result, the design of an online implementation of the methods described herein is presently underway with the purpose of providing the LHC operators with either continuous or on-demand chromaticity measurements.

ACKNOWLEDGMENTS

The authors acknowledge the stimulating discussions with O. R. Jones and T. Lefèvre, as well as the assistance of T. Argyropoulos, T. Levens, O. Marquerssen, and M. Wendt.

APPENDIX: DIPOLE MOMENT SIGNAL

The dipole moment signal due to a single-particle i can be given in the following form:

$$D^i(t) \propto I_i(t) \cdot x_i(t),$$

where $I_i(t)$ is the intensity signal and by $x_i(t)$ we denote the transverse displacement. According to Ref. [15], we have

$$I_i(t) \propto \text{Re} \left(\sum_{n=-\infty}^{\infty} e^{jn\omega_0[t + \widehat{\tau}_i \sin(\Omega_{s_i}t + \varphi_{s_i})]} \right),$$

where ω_0 is the revolution frequency and $\widehat{\tau}_i$, Ω_{s_i} , and φ_{s_i} are, respectively, the amplitude, the frequency, and the initial phase of a synchrotron motion. Assuming a constant betatron amplitude \widehat{x} , we can write

$$x_i(t) = \widehat{x} \cos[\phi_{\beta_i}(t)],$$

where ϕ_{β_i} is the phase of the betatron oscillations.

The betatron frequency of particle i is given by the product of betatron tune $Q_i(t)$ and the nominal revolution frequency ω_0 :

$$\omega_{\beta_i}(t) = Q_i(t)\omega_0,$$

which, as a consequence of the synchrotron motion, can be expressed by

$$\omega_{\beta_i}(t) = [Q + \widehat{Q}_i \cos(\Omega_{s_i}t + \varphi_{s_i})]\omega_0, \quad (\text{A1})$$

where Q is the nominal tune and \widehat{Q}_i is the amplitude of the tune oscillations. A convention here is adopted such that the amplitude of synchrotron motion $\widehat{\tau}_i$ is positive, whereas the amplitude of momentum oscillations \widehat{p}_i and the amplitude of betatron tune oscillations \widehat{Q}_i may be of any sign, depending on signs of the slip factor η and chromaticity $Q\xi$.

Integrating Eq. (A1) with respect to time gives the phase of betatron motion:

$$\phi_{\beta_i}(t) = Q\omega_0 t + \frac{\widehat{Q}_i\omega_0}{\Omega_{s_i}} \sin(\Omega_{s_i}t + \varphi_{s_i}) + \varphi_{\beta_i}, \quad (\text{A2})$$

where φ_{β_i} is the initial phase of the betatron oscillation. Finally, the dipole moment reads as follows:

$$\begin{aligned} D^i(t) &\propto I_i(t) \cdot x_i(t) \\ &= \text{Re} \left(\sum_{n=-\infty}^{\infty} e^{jn\omega_0[t + \widehat{\tau}_i \sin(\Omega_{s_i}t + \varphi_{s_i})]} \right) \widehat{x} \cos[\phi_{\beta_i}(t)] \\ &= \frac{\widehat{x}}{2} \text{Re} \left(\sum_{n=-\infty}^{\infty} e^{jn\omega_0[t + \widehat{\tau}_i \sin(\Omega_{s_i}t + \varphi_{s_i})] \pm j\phi_{\beta_i}(t)} \right), \end{aligned}$$

where \pm denotes summation over both signs. If we expand $\phi_{\beta_i}(t)$ according to Eq. (A2), we can arrange the expression into three exponents:

$$D^i(t) \propto \text{Re} \left(\sum_{n=-\infty}^{\infty} e^{j(n\pm Q)\omega_0 t} e^{jn\widehat{\tau}_i \sin(\widehat{Q}_i/\Omega_{s_i})\omega_0} \sin(\Omega_{s_i}t + \varphi_{s_i}) e^{j\varphi_{\beta_i}} \right).$$

By virtue of the Jacobi-Angers expansion

$$e^{jz \sin \theta} = \sum_{p=-\infty}^{\infty} J_p(z) e^{jp\theta},$$

the second exponent may be transformed, and the summand takes the following form:

$$\sum_{p=-\infty}^{\infty} J_p \left[\left(n\widehat{\tau}_i \pm \frac{\widehat{Q}_i}{\Omega_{s_i}} \right) \omega_0 \right] e^{j\{t[(n\pm Q)\omega_0 + p\Omega_{s_i}] + \varphi_{\beta_i} + p\varphi_{s_i}\}}.$$

Assuming that the betatron frequency spread is due only to natural chromaticity, we have

$$\widehat{Q}_i = Q\xi \frac{\widehat{p}_i}{p_0},$$

where p_0 is the nominal momentum. We also have [see Eq. (7) in Ref. [30]] that

$$\widehat{\tau}_i = \frac{\eta}{\Omega_{s_i}} \frac{\widehat{p}_i}{p_0},$$

where the slip factor η is negative for machines operating above transition energy (such as the LHC).

We can now rewrite the argument of the Bessel function as

$$\chi_{i,n}^{\pm} := \left(n\widehat{\tau}_i \pm \frac{\widehat{Q}_i}{\Omega_{s_i}} \right) \omega_0 = (n\eta \pm Q\xi) \frac{\omega_0 \widehat{p}_i}{\Omega_{s_i} p_0}.$$

This gives us a compact form:

$$D^i(t) \propto \text{Re} \left(\sum_{n,p=-\infty}^{\infty} J_p(\chi_{i,n}^{\pm}) e^{j\{t[(n\pm Q)\omega_0 + p\Omega_{s_i}] + \varphi_{\beta_i} + p\varphi_{s_i}\}} \right).$$

It is important to note that the value of Q can be decomposed into its integer and fractional part: $Q = Q_I + Q_F$. If the integer part is not zero, transverse sidebands corresponding to the n th harmonic of the revolution frequency are, in fact, located around $n - Q_I$ and $n + Q_I$ harmonics. In order to derive an expression convenient for studying the spectrum around the given harmonic of the revolution frequency, we will transform the sum above by the following shift. For every summand, we replace the index n by $n \mp Q_I$ (the choice of sign is opposite to $\chi_{i,n}^{\pm}$). We can do so, as every summand remains included in the infinite sum. The dipole moment signal reads then as follows:

$$D^i(t) \propto \text{Re} \left(\sum_{n,p=-\infty}^{\infty} J_p(\chi_{i,n \mp Q_I}^{\pm}) e^{j\{t[(n\pm Q_F)\omega_0 + p\Omega_{s_i}] + \varphi_{\beta_i} + p\varphi_{s_i}\}} \right),$$

where the summand indexed by n describes the vicinity of the n th harmonic of the revolution frequency.

- [1] Fritz Caspers and D. Möhl, History of stochastic beam cooling and its application in many different projects, *Eur. Phys. J. H* **36**, 601 (2012).
- [2] A. Sukhanov, K. A. Brown, C. W. Dawson, J. P. Jamilkowski, A. Marusic, and J. Morris, Processing of the schottky signals at RHIC, in *Proceedings of the International Conference on Accelerator and Large Experimental Control Systems (ICALEPCS'17), Barcelona, Spain, 2017*, Number 16 in International Conference on Accelerator and Large Experimental Control Systems (JACoW, Geneva, 2018), pp. 1327–1329, [10.18429/JACoW-ICALEPCS2017-THMPA08](https://cds.cern.ch/record/254747?ln=en).
- [3] Ralph J. Pasquinelli and Andreas Jansson, Microwave Schottky diagnostic systems for the Fermilab Tevatron, Recycler, and CERN Large Hadron Collider, *Phys. Rev. Accel. Beams* **14**, 072803 (2011).
- [4] R. Singh, O. Boine-Frankenheim, O. Chorniy, P. Forck, R. Haseitl, W. Kaufmann, P. Kowina, K. Lang, and T. Weiland, Interpretation of transverse tune spectra in a heavy-ion synchrotron at high intensities, *Phys. Rev. Accel. Beams* **16**, 034201 (2013).
- [5] M. E. Castro, Friedhelm Caspers, T. Kroyer, R. Jones, Jean-Pierre Koutchouk, and G. Tranquille, Results from the SPS 1.7 GHz travelling wave schottky monitor, Report No. CERN-AB-2005-075, 2005.
- [6] Jacques Bossler, Report No. CERN-PS-95-028-BD, 1995.
- [7] Maria Elena Angoletta, V. Chohan, M. Ludwig, O. Marquersen, P. Odier, F. Pedersen, U. Raich, L. Søby, G. Tranquille, and T. Spickermann, Measurements on the low-intensity beams of LEAR and the antiproton accumulator, Report No. CERN-PS-2001-053-BD, 2001, revised version number 1.
- [8] Lars Søby, Maria Elena Angoletta, Marco Bau, Marco Ferrari, Vittorio Ferrari, Ricardo Marco-Hernandez, John Molendijk, Flemming Pedersen, and Jorge Sanchez-Quesada, Beam measurement systems for the CERN antiproton decelerator (AD), Report No. CERN-ACC-2015-307, MOPTY056, 2015.
- [9] M. Betz, O. R. Jones, T. Lefevre, and M. Wendt, Bunched-beam Schottky monitoring in the LHC, *Nucl. Instrum. Methods Phys. Res., Sect. A* **874**, 113 (2017).
- [10] Kacper Lasocha and Diogo Alves, Estimation of longitudinal bunch characteristics in the LHC using Schottky-based diagnostics, *Phys. Rev. Accel. Beams* **23**, 062803 (2020).
- [11] Oliver S. Bruning, W. Hofle, R. Jones, T. Linnecar, and H. Schmickler, Chromaticity measurements via RF phase modulation and continuous tune tracking, in *Proceedings of the 8th European Particle Accelerator Conference, Paris, 2002* (EPS-IGA and CERN, Geneva, 2002), pp. 1852–1854.
- [12] Arising, for example, from impedance-driven collective effects.
- [13] Trevor Paul R. Linnecar and Walter Scandale, A transverse Schottky noise detector for bunched proton beams, *IEEE Trans. Nucl. Sci.* **28**, 2147 (1981).
- [14] Swapan Chattopadhyay, *Some Fundamental Aspects of Fluctuations and Coherence in Charged-Particle Beams in Storage Rings*, CERN Yellow Reports: Monographs (CERN, Geneva, 1984).
- [15] Daniel Boussard, *Schottky Noise and Beam Transfer Function Diagnostics*, 1995 ed. (CERN, Geneva, 1995), <https://cds.cern.ch/record/254747?ln=en>.
- [16] Ondine Chanon, *Schottky Signal Analysis: Tune and Chromaticity Computation* (CERN, Geneva, 2016), <http://cds.cern.ch/record/2212811?ln=en>.
- [17] Michael Betz, Manfred Wendt, and Thibaut Lefevre, *Summary of LHC MD:377: Schottky Pick-Up* (CERN, Geneva, 2015), <http://cds.cern.ch/record/2110648>.
- [18] Friedhelm Caspers, *Schottky Signals for Longitudinal and Transverse Bunched-Beam Diagnostics* (CERN, Geneva, 2009), <https://cds.cern.ch/record/1213284>.
- [19] Stefan Paret, Vladimir Kornilov, Oliver Boine-Frankenheim, and Thomas Weiland, Transverse Schottky and beam transfer function measurements in space charge affected coasting ion beams, *Phys. Rev. Accel. Beams* **13**, 022802 (2010).
- [20] Simon van der Meer, Diagnostics with Schottky noise, in *Proceedings of the 3rd Joint U.S.–CERN School on Particle Accelerators: Frontiers of Particle Beams, Observation, Diagnosis and Correction* (Springer, Berlin, 1988), pp. 423–433, <https://cds.cern.ch/record/113954>.
- [21] A. Jansson, P. Lebrun, and R. Pasquinelli, Experience with the 1.7 GHz schottky pick-ups in the tevatron, in *Proceedings of the 9th European Particle Accelerator Conference, Lucerne, 2004* (EPS-AG, Lucerne, 2004), pp. 2777–2779.
- [22] Laurent Schwartz, *Théorie des Distributions, t. 1–2* (Hermann, Paris, 1951).
- [23] W. N. Bailey, Some series of squares of Bessel functions, *Math. Proc. Cambridge Philos. Soc.* **26**, 82 (1930).
- [24] A. Abdi, C. Tepedelenlioglu, M. Kaveh, and G. Giannakis, On the estimation of the k parameter for the Rice fading distribution, *IEEE Commun. Lett.* **5**, 92 (2001).
- [25] Eric Jones, Travis Oliphant, Pearu Peterson *et al.*, SciPy: Open source scientific tools for Python, 2001, online; accessed May 16, 2022.
- [26] Richard H. Byrd, Peihuang Lu, Jorge Nocedal, and Ciyong Zhu, A limited memory algorithm for bound constrained optimization, *SIAM J. Sci. Comput.* **16**, 1190 (1995).
- [27] Elena Shaposhnikova, Taylor Bohl, and T. Linnecar, Longitudinal peak detected Schottky spectrum (2010), pp. 363–367.
- [28] F. Tecker, Longitudinal beam dynamics, [arXiv:1601.04901](https://arxiv.org/abs/1601.04901).
- [29] For example, in the presence of coherent intrabunch motion, which not only distorts the longitudinal spectrum, but also heavily complicates the relation between the bunch profile and the distribution of synchrotron amplitudes.
- [30] J. L. Laclare, *Bunched Beam Coherent Instabilities* (CERN, Geneva, 1987), <https://cds.cern.ch/record/611596>.